Two-dimensional compressible viscous flow around a circular cylinder

Daniel Canuto[1],[‡] and Kunihiko Taira[1],[†]

[1]Department of Mechanical Engineering, Florida A&M/Florida State University,
Tallahassee, FL 32310, USA

Direct numerical simulation is performed to study compressible viscous flow around a circular cylinder. The present study considers two-dimensional shock-free continuum flow by varying the Reynolds number between 20 and 100 and the free-stream Mach number between 0 and 0.5. The results indicate that compressibility effects elongate the near wake for cases above and below the critical Reynolds number for two-dimensional flow under shedding. The wake elongation becomes more pronounced as the Reynolds number approaches this critical value. Moreover, we determine the growth rate and frequency of linear instability for cases above the critical Reynolds number. From the analysis, it is observed that the frequency of the Bénard–von Kármán vortex street in the time-periodic fully saturated flow increases from the dominant unstable frequency found from the linear stability analysis as the Reynolds number increases from its critical value, even for the low range of Reynolds numbers considered. We also find that the compressibility effects reduce the growth rate and dominant frequency in the linear growth stage. Semi-empirical functional relationships for the growth rate and the dominant frequency in linearized flow around the cylinder in terms of the Reynolds number and free-stream Mach number are presented.

Key words: compressible flows, instability, wakes

1. Introduction

Fluid flow around bluff bodies is one of the important flows that has been extensively studied in the field of fluid mechanics. As a basic model for such flows, and with a wide range of engineering applications in its own right, the flow over a circular cylinder has garnered much interest. The beginning of this deluge of research can be traced back to the late nineteenth and early twentieth centuries, and is due to researchers such as Strouhal (1878), Rayleigh (1879), Bénard (1908) and von Kármán (1911).

It is well-known that incompressible flow over a circular cylinder can be characterized by the free-stream Reynolds number $Re \equiv \rho_\infty u_\infty d / \mu_\infty$, where ρ_∞ is the free-stream density, u_∞ is the free-stream velocity, d is the cylinder diameter

† Email address for correspondence: ktaira@fsu.edu
‡ Present address: Department of Mechanical and Aerospace Engineering,
University of California, Los Angeles, CA 90095, USA.

and μ_∞ is the free-stream dynamic viscosity. For a range of Re from around 5 to 47, the separated flow behind the cylinder forms a steady and symmetric closed wake. The variation in wake geometry with Re in this regime has been investigated in great depth for incompressible flow by Taneda (1956), Coutanceau & Bouard (1977) and Fornberg (1980), among others.

As Re is increased beyond around 47, the flow exhibits two-dimensional periodic laminar shedding of wake vortices. This regime persists up to the onset of spanwise instabilities at $Re \approx 190$ (Williamson 1988*b*; Behara & Mittal 2010), and is characterized by the alternate shedding of two-dimensional vortices from the top and bottom halves of the cylinder. For $Re \gtrsim 190$, spanwise variation can be observed while the shedding of the vortices remains nominally two-dimensional. This shedding phenomenon is the well-known Kármán (Bénard–von Kármán) vortex street. Since its first experimental observation by Mallock (1907) and Bénard (1908), a large body of work has been dedicated to its characterization. For instance, the practical importance of quantifying the unsteady loads generated by the vortex street has motivated unsteady lift and drag force measurements over a range of Re from the onset of two-dimensional oscillation ($Re \approx 47$) up to and past the point at which the boundary layer becomes fully turbulent ($Re \approx 2 \times 10^6$) (Fung 1960; Gerrard 1961; Bishop & Hassan 1964; Sanada & Matsumoto 1992; Norberg 2001). Here, it is worth noting that the mean drag force has also been measured over a similar range of Re (Wieselsberger 1921; Delany & Sorenson 1953; Finn 1953; Tritton 1959; Roshko 1961) as a consequence of its significance in aerodynamics. From these measurements, it has been observed that the mean drag coefficient per unit span $C_d \equiv F_d/(\rho_\infty u_\infty^2 d/2)$ (where F_d is the mean drag force) remains relatively constant for $10^3 \lesssim Re \lesssim 10^5$, and that a drastic drop in C_d (known as the 'drag crisis') occurs at $Re \approx 2 \times 10^5$ as a consequence of delayed separation caused by the boundary layer transition to turbulence.

In addition to force measurements, a number of studies have also focused on the influence of Re on the shedding frequency. A partial listing of some of the important work performed in this vein includes Roshko (1954), Tritton (1959) and Williamson (1988*a*). Besides determining the vortex-shedding frequency, past research has also been concerned with the analysis of its stability. Such an analysis was first performed by von Kármán (1911) for point vortices, and studies of a similar nature were performed for finite-cored vortices by Saffman & Schatzman (1982) and Meiron, Saffman & Schatzman (1984). These works were concerned with the determination of stable configurations for developed vortex streets, and were not intended to uncover a mechanism for the emergence of instability. Marsden & McCracken (1976) provided the first suggestion of such a mechanism, explaining that the wake transitioning from flow with steady recirculation to that with periodic two-dimensional shedding could be understood as a Hopf bifurcation from a stable fixed point to a stable closed orbit. Provansal, Mathis & Boyer (1987) expanded on this idea, modelling the flow as a dynamical system described by the Stuart–Landau equation, given by

$$\frac{\mathrm{d}A}{\mathrm{d}t} = \sigma A - \frac{1}{2}l|A|^2 A, \tag{1.1}$$

where A is a complex-valued function of time, $\sigma = \sigma_r + \mathrm{i}\sigma_i$ is a global constant of the flow that corresponds to an eigenvalue of the linearized Navier–Stokes operator, and $l = l_1 + \mathrm{i}l_2$ is a spatially varying parameter related to the deformation of the mode in space as it is amplified in time (Dušek, Le Gal & Fraunié 1994). Under

this model, A can be any flow variable that undergoes oscillation, and is often taken as the transverse velocity u_y in the literature. For a given mode, $\sigma_r > 0$ is the necessary condition for infinitesimal disturbances to be amplified. This condition also corresponds to $Re > Re_c$, for which the flow is referred to as the unstable regime in this study. In recent times, variations of the Stuart–Landau equation have been used by Noack *et al.* (2003), Sipp & Lebedev (2007) and Sengupta, Singh & Suman (2010) to model the spatial and temporal evolution of flow instabilities. Other modern advancements in stability analysis of two-dimensional incompressible flow around a circular cylinder include the experimental determination of σ_r (Strykowski & Sreenivasan 1990), the location of both the instability core and regions of high sensitivity to perturbations (Giannetti & Luchini 2007), and the isolation of the antisymmetric modes that give rise to further instabilities at higher Re (Kumar *et al.* 2009). As can be seen from the above discussion, the wake geometry at stable Re, the transient behaviour of the flow as it transitions from a steady closed wake to a two-dimensional vortex street and the fully developed laminar vortex street have been investigated quite extensively for incompressible flow.

Considering the significant accumulation of knowledge on incompressible flow around a circular cylinder, comparatively little attention has been paid to the effects of compressibility on the behaviour of the wake in these low-Re flow regimes. While a limited number of studies have examined the effects of compressibility on the flow around a circular cylinder, these studies were undertaken at Re on the order of 10^5, four orders of magnitude higher than Re_c (Lindsey 1937; Macha 1977; Zdravkovich 1997). This lack of fundamental studies in low-Re compressible flows may have been due to a historical dearth of engineering applications in such regimes. However, fields are now emerging in which compressible low-speed flows play an integral role. For example, the design of small-scale aircraft for low-density environments, such as those seen on Mars or at ultra-high altitudes on Earth, requires an understanding of such flows. Basic aerodynamic information in these areas is currently limited but is starting to be compiled (Drela 1992; Okamoto 2005; Suwa *et al.* 2012; Nagai *et al.* 2013; Munday *et al.* 2015). Another example is the optimization of liquid atomization, where micro-sized droplets travelling at relatively high speeds are formed. While the overall flow is a complex multiphase problem (Gorokhovski & Herrmann 2008; Shinjo & Umemura 2010), the behaviour of these droplets and other small structures is partially a consequence of compressibility effects at low Re. It is thus evident that in order to expand the horizon of fluid mechanics applications, a fundamental knowledge of low-Re compressible flow is necessary.

The present study employs two-dimensional direct numerical simulation (DNS) in an attempt to fill this gap in our knowledge of the effects of compressibility on the two-dimensional viscous flow around a circular cylinder at Reynolds numbers near the onset of two-dimensional shedding. In particular, we aim to uncover these effects with respect to the characteristic parameters of steady wakes, the dominant frequency of shedding wakes, and the primary wake instability that causes a transition between the two wake types for $Re > Re_c \approx 47$. Such knowledge will be useful not only for gaining a deeper comprehension of this fundamental flow, but also for validation of compressible flow solvers and stability analysis.

In what follows, we describe the problem of interest and discuss the findings from the present study. The computational setup, numerical method and validation are discussed in §2. The results based on the computation are presented in §3, where we illustrate the influence of compressibility on the wake behind a circular cylinder. Findings from compressible flow near the onset of shedding are presented. Also

discussed in detail are the characteristics of the shedding instability that appears for $Re > Re_c$ and the effects of compressibility on these properties. To complement this discussion, semi-empirical relationships for the growth rate and dominant unstable frequency at the onset of this instability in terms of Re and free-stream Mach number M_∞ are presented. Concluding remarks are offered in §4.

2. Simulation approach

2.1. *Problem description*

The present investigation numerically examines the two-dimensional compressible viscous flow around a circular cylinder. The governing equations for this flow are the full compressible Navier–Stokes equations:

$$\frac{\partial \hat{\rho}}{\partial \hat{t}} + \frac{\partial}{\partial \hat{x}_j}(\hat{\rho}\hat{u}_j) = 0, \tag{2.1}$$

$$\frac{\partial(\hat{\rho}\hat{u}_i)}{\partial \hat{t}} + \frac{\partial}{\partial \hat{x}_j}(\hat{\rho}\hat{u}_i\hat{u}_j + \hat{p}\delta_{ij}) = \frac{1}{Re_{a_\infty}}\frac{\partial}{\partial \hat{x}_j}\left(\frac{\partial \hat{u}_i}{\partial \hat{x}_j} + \frac{\partial \hat{u}_j}{\partial \hat{x}_i} - \frac{2}{3}\frac{\partial \hat{u}_k}{\partial \hat{x}_k}\delta_{ij}\right), \tag{2.2}$$

$$\frac{\partial \hat{e}}{\partial \hat{t}} + \frac{\partial}{\partial \hat{x}_j}\left[(\hat{e}+\hat{p})\hat{u}_j\right] = \frac{1}{Re_{a_\infty}}\frac{\partial}{\partial \hat{x}_j}\left[\hat{u}_i\left(\frac{\partial \hat{u}_i}{\partial \hat{x}_j} + \frac{\partial \hat{u}_j}{\partial \hat{x}_i} - \frac{2}{3}\frac{\partial \hat{u}_k}{\partial \hat{x}_k}\delta_{ij}\right)\right] + \frac{1}{Re_{a_\infty}}\frac{1}{Pr}\frac{\partial^2 \hat{T}}{\partial \hat{x}_k \partial \hat{x}_k}, \tag{2.3}$$

where variables with a hat (e.g. $\hat{\rho}$) have been non-dimensionalized according to

$$\hat{\rho} = \frac{\rho}{\rho_\infty}, \quad \hat{p} = \frac{p}{\rho_\infty a_\infty^2}, \quad \hat{T} = \frac{T}{T_\infty}, \quad \hat{e} = \frac{e}{\rho_\infty a_\infty^2}, \tag{2.4a–d}$$

$$\hat{u}_i = \frac{u_i}{a_\infty}, \quad \hat{x}_i = \frac{x_i}{d}, \quad \hat{t} = \frac{ta_\infty}{d}. \tag{2.4e–g}$$

Here, a_∞ is the free-stream sonic speed, ρ_∞ is the free-stream density, T_∞ is the free-stream temperature, and d is the cylinder diameter. Note that the origin of the spatial coordinate system is placed at the centre of the cylinder. The dimensionless parameters that appear in the governing equations are the acoustic Reynolds number and Prandtl number, given by

$$Re_{a_\infty} \equiv \frac{\rho_\infty a_\infty d}{\mu_\infty} \quad \text{and} \quad Pr = \frac{\mu_\infty}{\rho_\infty \alpha_\infty}, \tag{2.5a,b}$$

respectively, where μ_∞ is the free-stream dynamic viscosity and α_∞ is the free-stream thermal diffusivity. In this study, the flow fields are specified by the Mach number and convective Reynolds number, defined as

$$M_\infty \equiv \frac{u_\infty}{a_\infty} \quad \text{and} \quad Re \equiv \frac{\rho_\infty u_\infty d}{\mu_\infty} = Re_{a_\infty} M_\infty, \tag{2.6a,b}$$

respectively, where u_∞ is the free-stream velocity. The ranges of Reynolds number and Mach number considered in this study are $20 \leqslant Re \leqslant 100$ and $0 \leqslant M_\infty \leqslant 0.5$, respectively, with $M_\infty = 0$ representing the incompressible limit of the flow. These values are chosen to examine the influence of Mach number on the wake and the

emergence of instability. Throughout the study, we use $\gamma = 1.4$ for the specific heat ratio, representative of air.

The forces on the cylinder are reported in terms of the drag and lift coefficients per unit span:

$$C_d \equiv \frac{F_d}{\frac{1}{2}\rho_\infty u_\infty^2 d} \quad \text{and} \quad C_l \equiv \frac{F_l}{\frac{1}{2}\rho_\infty u_\infty^2 d}, \qquad (2.7a,b)$$

where F_d and F_l are the sectional drag and lift forces, respectively. In the following discussion, an overbar ($^-$) on these coefficients indicates a time-averaged value, while a prime ($'$) denotes a single-sided fluctuation amplitude. The pressure is non-dimensionalized as the coefficient of pressure using the far-field dynamic pressure

$$C_p \equiv \frac{p - p_\infty}{\frac{1}{2}\rho_\infty u_\infty^2}. \qquad (2.8)$$

To analyse periodic shedding in the unstable regime after the flow has reached its limit cycle, we use Strouhal number as the non-dimensional frequency:

$$St \equiv \frac{fd}{u_\infty}, \qquad (2.9)$$

where f is the dimensional shedding frequency.

The range of Knudsen number $Kn = \sqrt{\pi\gamma/2}M_\infty/Re$ for the cases considered in this study is 0–0.037 (with the maximum Kn occurring for the case of $M_\infty = 0.5$ and $Re = 20$). Since Kn characterizes the ratio of the molecular mean free path to the characteristic length, the continuum assumption may be applied for $Kn \ll 1$. In the present study, we therefore treat the flow as a continuum with no-slip applied at the cylinder surface (Bird 1994). While there may be some molecular effects that can contribute to the flow physics, we limit the current investigation to examining the compressibility effects on the cylinder wake and its stability properties in the context of a continuum.

2.2. *Numerical method*

For the present study, we perform DNS using the compressible flow solver CharLES, developed by Cascade Technologies, Inc. A detailed description of the code is provided in Khalighi *et al.* (2011) and Brés *et al.* (2012). CharLES uses a second-order-accurate finite-volume method in conjunction with a third-order Runge–Kutta time integration scheme. Extensive validation using this solver has been performed for compressible flows over bodies at low to moderate Re.

The computational domain in this study is chosen to be sufficiently large with a dimension of $(x/d, y/d) \in [-20, 40] \times [-20, 20]$, as shown in figure 1. The flow is prescribed to be uniform at the inlet $\boldsymbol{u}/u_\infty = (1, 0)$ with free-stream values of non-dimensional density and pressure being specified as 1 and $1/\gamma$, respectively. Along the outlet, a sponge zone is applied for the exiting wake vortices to be damped out without affecting the near-field solution (Freund 1997). For the top and bottom boundaries, symmetry boundary conditions are specified. On the cylinder surface, we prescribe no-slip and adiabatic boundary conditions. To ensure stability of the method, the CFL number, defined as $CFL = a_\infty \Delta t / \Delta x_{min}$, is limited to 1, where Δx_{min} is the minimum streamwise grid spacing and Δt is the time step.

To test the validity of our computational setup, grid resolution and domain size were examined. Owing to the availability of reference conditions, the validation conditions
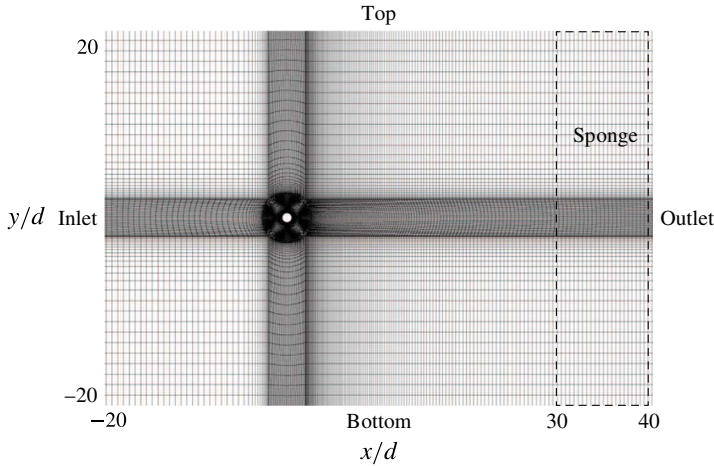
FIGURE 1. Representative computational domain used for this study.

Grid size	$\overline{C}_d$	$\Delta\overline{C}_d$	C_l'	$\Delta C_l'$
Baseline (9.2×10^4 points)	1.378	0.073 %	0.325	−0.612 %
Refined (1.9×10^6 points)	1.377	—	0.327	—

TABLE 1. Computed drag and lift coefficients from a grid refinement study for $Re = 100$ and $M_\infty = 0.25$. The differences, $\Delta\overline{C}_d$ and ΔC_l, are calculated as the difference from the refined case.

Grid size	$\overline{C}_d$	$\Delta\overline{C}_d$	C_l'	$\Delta C_l'$
Baseline $((x/d, y/d) \in [-20, 40] \times [-20, 20])$	1.350	0.521 %	0.329	−0.604 %
Large $((x/d, y/d) \in [-20, 60] \times [-40, 40])$	1.343	—	0.331	—

TABLE 2. Computed drag and lift coefficients from a domain size study for $Re = 100$ and $M_\infty = 0.05$. The differences, $\Delta\overline{C}_d$ and ΔC_l, are calculated as the difference from the baseline case.

were chosen to be $Re = 100$ and $M_\infty = \{0.05, 0.25\}$. The C_d and C_l values obtained from the grid refinement study are shown in table 1. From these results, it can be observed that the baseline grid provides sufficient resolution. Using the same baseline grid, the changes in C_d and C_l due to variation in domain size are displayed in table 2. These results indicate that our baseline computational domain is sufficiently large to prevent the computational boundaries from influencing the flow near the cylinder.

Incompressible and compressible flows were simulated on the baseline setup and compared with those reported in several other studies (Tritton 1959; Coutanceau & Bouard 1977; Linnick & Fasel 2005; Taira & Colonius 2007; Karagiozis, Kamakoti & Pantano 2010). The results of validation for different flows are shown in table 3, where the characteristic wake properties l_r, l_a, l_b and θ_s are defined in figure 2. From the comparison, it can be seen that the baseline grid and computational domain size are in good agreement with previous work for flows both above and below the critical

Re	M_∞	References	l_r/d	l_a/d	l_b/d	θ_s (deg.)	$\overline{C}_d$	C_l'	St
20	0	Coutanceau & Bouard (1977)	0.93	0.33	0.46	45.0	—	—	—
		Tritton (1959)	—	—	—	—	2.09	—	—
		Linnick & Fasel (2005)	0.93	0.36	0.43	43.5	2.06	—	—
		Taira & Colonius (2007)	0.94	0.37	0.43	43.3	2.06	—	—
		Present	0.92	0.36	0.42	43.7	2.07	—	—
40	0	Coutanceau & Bouard (1977)	2.13	0.76	0.59	53.8	—	—	—
		Tritton (1959)	—	—	—	—	1.59	—	—
		Linnick & Fasel (2005)	2.28	0.72	0.60	53.6	1.52	—	—
		Taira & Colonius (2007)	2.30	0.73	0.60	53.7	1.54	—	—
		Present	2.24	0.72	0.59	53.7	1.54	—	—
100	0.05	Karagiozis *et al.* (2010)	—	—	—	—	1.317	0.320	0.168
		Present	—	—	—	—	1.350	0.329	0.167
100	0.25	Karagiozis *et al.* (2010)	—	—	—	—	1.336	0.319	0.168
		Present	—	—	—	—	1.378	0.325	0.163

TABLE 3. Comparison between present characteristic wake properties and values obtained from past studies. See figure 2 for definitions of l_r, l_a, l_b and θ_s.
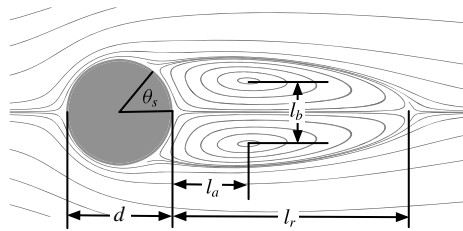

FIGURE 2. Characteristic wake properties for steady flow behind a circular cylinder.

transition for two-dimensional shedding ($Re_c \approx 47$ for $M_\infty = 0$ in this study). The baseline setup is hence used for the remainder of the study.

3. Compressible flow over a circular cylinder

In this section, we first focus our attention on the flow-field characteristics of stable and unstable flows. We then revisit the emergence of instability with linear stability analysis. Stable flows are defined for $Re < Re_c$ and the flow is steady. On the other hand, for unstable flows, we have $Re > Re_c$ and the flow exhibits unsteady vortex shedding. In our study, $Re_c \approx 47$ for the incompressible limit, though the following discussion will show that this value exhibits a slight sensitivity to M_∞.

3.1. *Flow physics*

We first examine the effect of compressibility on the characteristic closed wake dimensions for stable flows. Shown in figure 3 are contours of normalized velocity magnitude $\|\boldsymbol{u}\|/u_\infty$ in the near field of the cylinder. These flow fields indicate that the wake elongates as M_∞ is increased from 0 to 0.5. A similar trend has been established
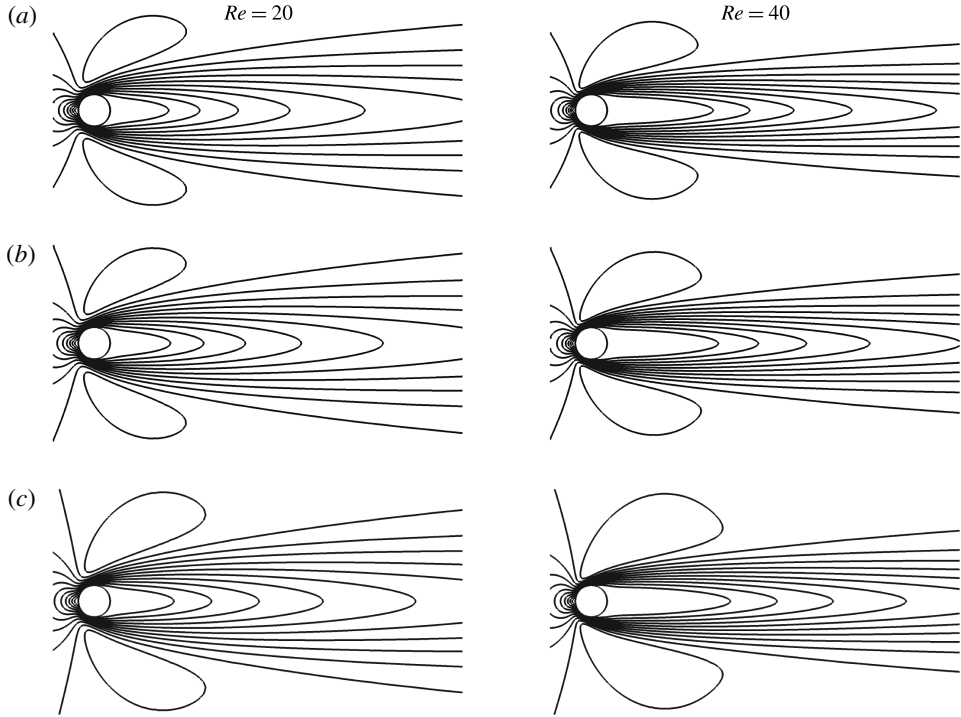
FIGURE 3. $\|\boldsymbol{u}\|/u_\infty$ for varying M_∞ ((*a*) 0, (*b*) 0.3, (*c*) 0.5) at stable *Re*. Contours are from 0 to 1.1 across 12 levels, and flow is from left to right.

in the literature for incompressible flows with increasing *Re* (Coutanceau & Bouard 1977). To further investigate the influence of compressibility on the wake, normalized wake geometry parameters are presented as functions of M_∞ for various stable *Re* in figure 4. From these measurements, it can be seen that the wake increases in length (as measured by l_r/d). It is also notable that over the range of M_∞ examined, the variation in l_a/d and l_r/d relative to their incompressible values is more than twice as large at $Re = 40$ as at $Re = 20$. This result indicates that as *Re* moves further away from Re_c, the wake becomes less susceptible to compressibility effects for stable flows. A similar result is obtained in terms of *St* for unstable flows and is discussed in further detail later in this section.

Based on observations from the steady wakes given in figures 3 and 4, it is expected that $\overline{C}_d$ should increase along with M_∞, as the wake exhibits a clear increase in size. This expectation is further justified by the previous observation of such behaviour for airfoils in similar flow conditions (Munday *et al.* 2015). Indeed, as shown in figure 5, we observe an increase in $\overline{C}_d$ as M_∞ increases. To supplement the explanation for this variation in $\overline{C}_d$ given by the wakes, we present distributions of C_p along the cylinder surface for selected cases in figure 6. From these distributions, we find that as M_∞ increases, the pressure along the front half of the cylinder (i.e. $\theta < 90°$) increases while the pressure at the rear stagnation point decreases. When coupled with the aforementioned shift in wake geometry, this increase in the pressure gradient between the upstream and downstream halves of the cylinder explains the observed rise in $\overline{C}_d$ with M_∞ for stable cases.
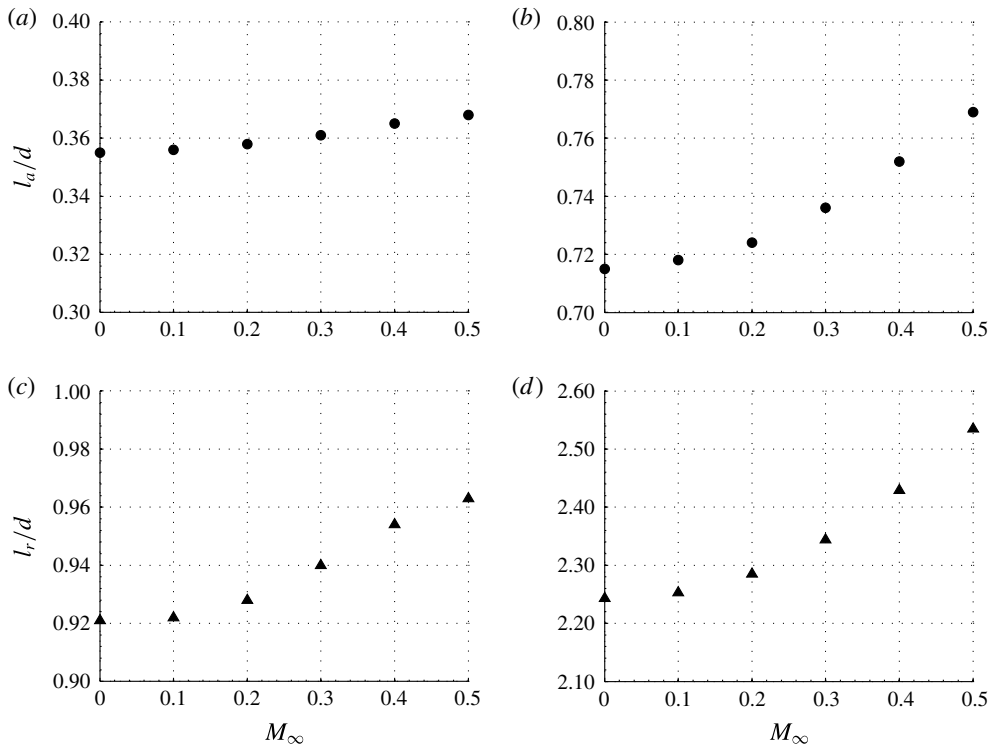
FIGURE 4. Wake characteristics for $0 \leqslant M_\infty \leqslant 0.5$, and $Re = 20$ (*a,c*) and 40 (*b,d*) (steady flow).

Interestingly, in comparing $\overline{C}_d$ for stable and unstable cases, we find that both classes of flow exhibit quadratic variations with M_∞, as indicated by the solid lines in figure 5. To explain this behaviour for unstable cases, we examine the flow fields obtained at $Re = 50$ for varying M_∞ in figure 7. From the contours of time-averaged velocity magnitude $\|\overline{\boldsymbol{u}}\|/u_\infty$, it can be seen that the effect of increasing M_∞ is to increase the size of the time-averaged recirculation region. This effect matches the increase in wake size with M_∞ previously displayed in figure 3 for stable flows, and thus explains the parallel trends in $\overline{C}_d$.

It is worth mentioning that the trends in $\overline{C}_d$ behave similarly to the well-known Prandtl–Glauert transformation (Glauert 1928). While this transform holds only for the lift force in inviscid flow, we observe that for higher-Reynolds-number flows in this study, the Prandtl–Glauert-type transformation is also able to approximate the drag force for compressible flow based on incompressible drag values

$$C_d = \frac{C_{d,M_\infty=0}}{\sqrt{1 - M_\infty^2}} = C_{d,M_\infty=0}\left(1 + \frac{1}{2}M_\infty^2 + \frac{3}{8}M_\infty^4 + \cdots\right), \tag{3.1}$$

as shown in figure 5 by the dashed lines. It is expected that the Prandtl–Glauert transformation would not accurately predict the compressibility effects on a cylinder since the transformation is also based on small deflections of the free stream as it flows over a slender body. However, the data appear to approach the theoretical trend
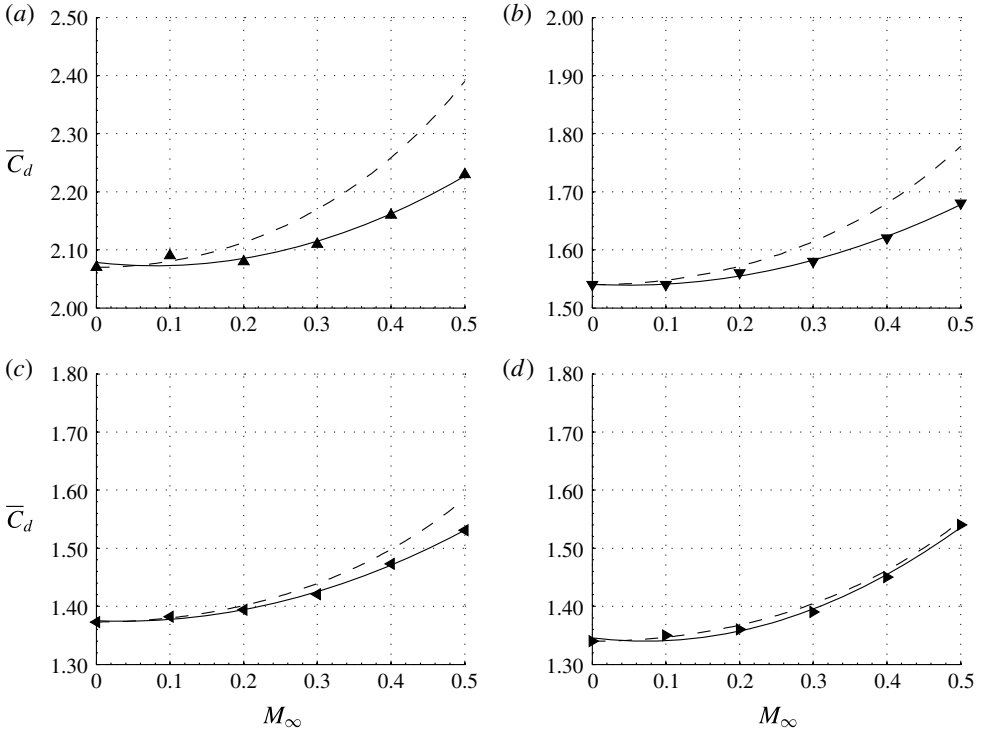
FIGURE 5. Drag coefficient $\overline{C}_d$ for selected stable and unstable cases. Overlaid solid lines are quadratic curve fits of the present data, while the dashed lines are the prediction given by the Prandtl–Glauert transformation. $Re = 20$ (*a*), 40 (*b*), 75 (*c*), 100 (*d*).
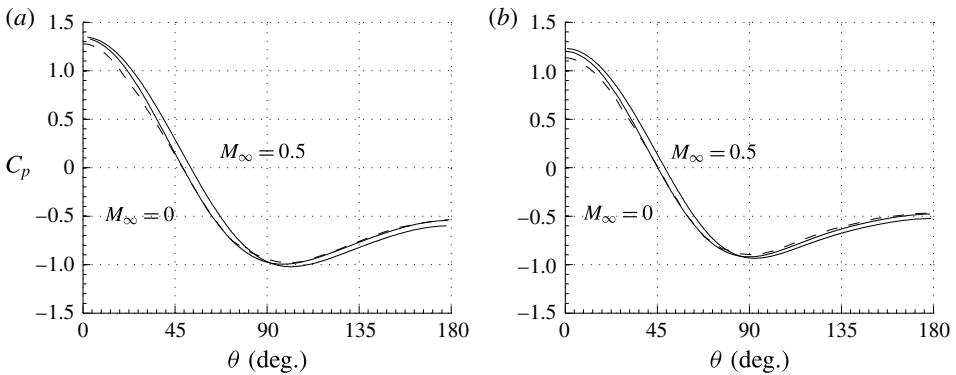

FIGURE 6. C_p distributions over the cylinder surface. Solid lines are from the present study. Overlaid dashed lines are the incompressible solutions from Fornberg (1980). $Re = 20$ (*a*), 40 (*b*).

with increasing Re (e.g. $Re = 100$). We attribute this result to the fact that the Prandtl–Glauert-type transformation performs well for flows at higher Re, for which viscous effects are of small magnitude compared to pressure effects.
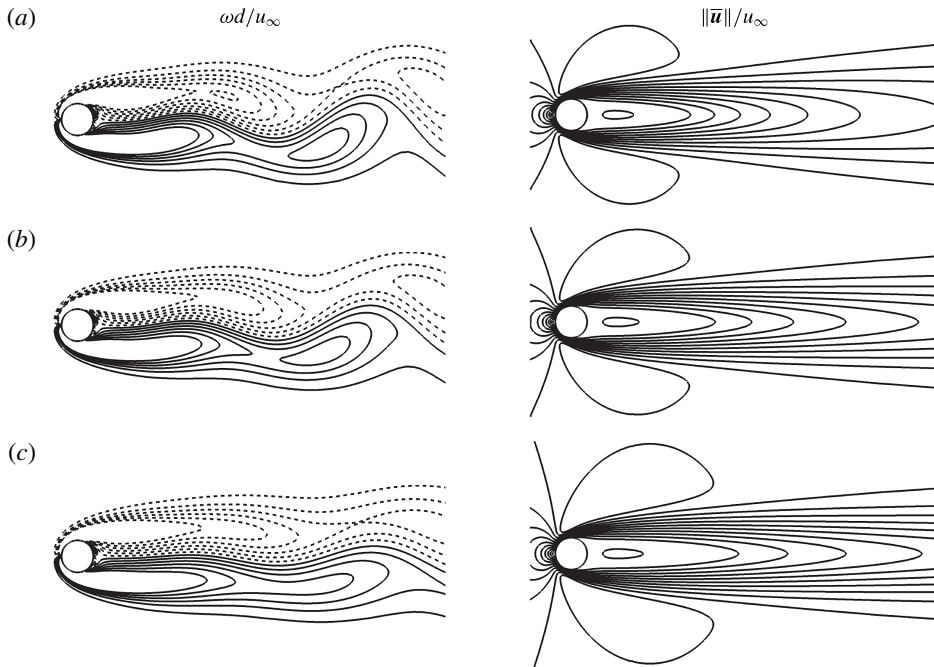
FIGURE 7. Flow-field comparisons for varying M_∞ ((a) 0, (b) 0.3, (c) 0.5) at $Re = 50$. Vorticity contours have 12 levels between $\pm M_\infty$, with dashed lines indicating negative values. Time-averaged velocity contours have 12 levels between 0 and 1.1.

Though our discussion up to this point has focused on the effects of compressibility on steady or time-averaged observations, changes in M_∞ are also reflected in unsteady flow phenomena. For instance, the snapshots of non-dimensionalized spanwise vorticity $\omega d/u_\infty$ in figure 7 indicate that compressibility tends to increase the wavelength of vortex shedding, thus leading to the aforementioned elongation of the time-averaged recirculation region. Besides the shedding wavelength, the effect of M_∞ on shedding frequency can be seen in figure 8, which shows the Strouhal number St as a function of M_∞ for different Re. From this plot, it is evident that increasing M_∞ reduces the frequency of vortex shedding. This trend matches the increase in vortex-shedding wavelength previously mentioned. Moreover, we see that the data show a smaller change in St from $M_\infty = 0$ to 0.5 as Re is increased beyond Re_c, with over a 9 % reduction at $Re = 50$, but only about 4 % at both $Re = 75$ and 100. This result indicates that St exhibits reducing sensitivity to compressibility effects as (Re–Re_c) increases. However, we have only made this observation for $47 \leqslant Re \leqslant 100$. Further investigation is needed to determine whether it holds up to and beyond the limit for spanwise instability ($Re \approx 190$) (Williamson 1996). Nonetheless, it is notable that this behaviour parallels that already discussed for the characteristic wake parameters in stable flow.

Finally, to isolate the effects of varying Re above Re_c for flows above the incompressible limit ($M_\infty \approx 0.3$), figure 9 shows the non-dimensionalized spanwise vorticity $\omega d/u_\infty$ and velocity magnitude $\|\overline{u}\|/u_\infty$ for different Re at $M_\infty = 0.5$. From the flow fields, it can be seen that with increasing Re, both the vortex-shedding
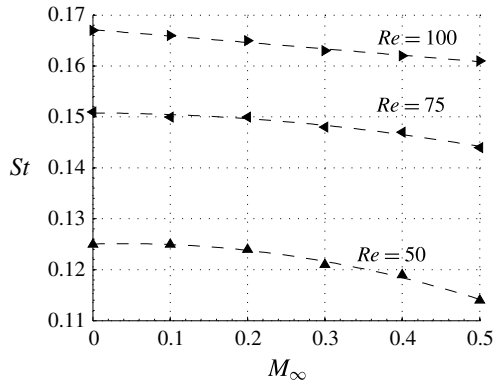
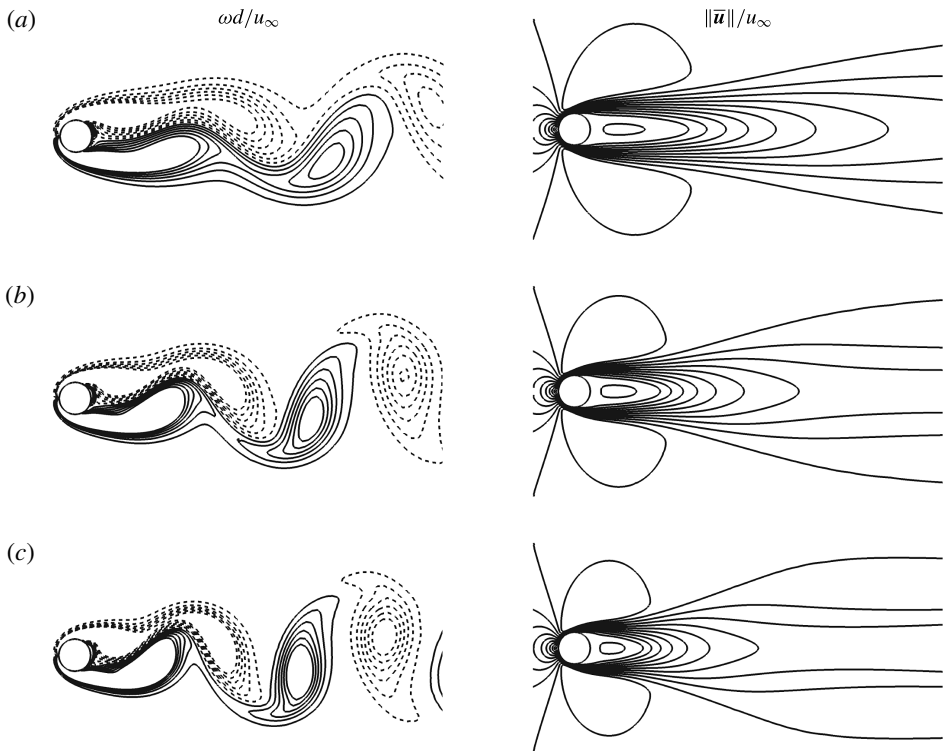FIGURE 8. *St* as a function of M_∞ for various unstable *Re*.

FIGURE 9. Flow-field comparisons for varying *Re* ((*a*) 60, (*b*) 80, (*c*) 100) at $M_\infty = 0.5$. Vorticity contours have 12 levels between $\pm M_\infty$, with dashed lines indicating negative values. Time-averaged velocity contours have 12 levels between 0 and 1.1.

length and the time-averaged recirculation region shorten. This trend has already been well-established for unsteady incompressible flows near Re_c (Coutanceau & Bouard 1977), and is now shown here to hold above the incompressible limit as well.
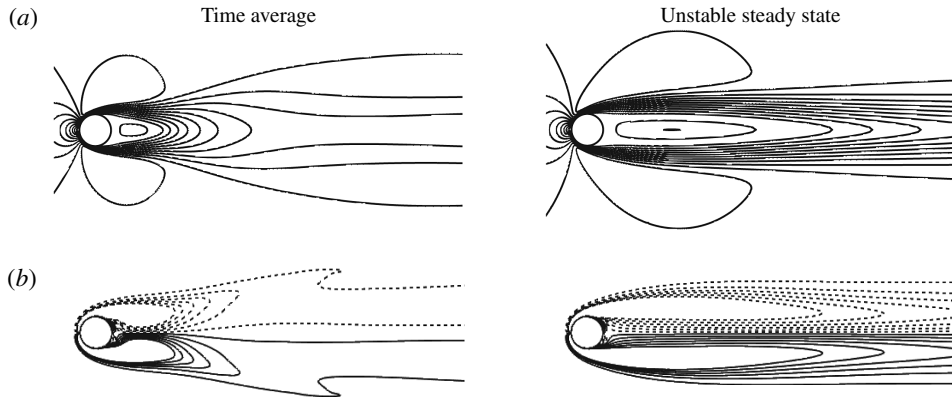
FIGURE 10. Comparison of velocity and vorticity fields for the time-averaged flow and unstable steady states for $Re = 100$ and $M_\infty = 0$. (a) $= \|\overline{\boldsymbol{u}}\|/u_\infty$, (b) $= \omega d/u_\infty$. Contour settings follow figures 9 and 7.

3.2. *Linear stability analysis*

The generation of wake vortices and the vortex street that appears in unstable flow over a circular cylinder gives rise to unsteady forces. To better understand the formation of the vortex street in compressible flow, we examine the growth of linear instability for unstable flows.

To perform linear stability analysis, we first find the base state from which to perturb the flow. The unstable steady state is used as the base state and is numerically determined for each combination of $Re > Re_c$ and M_∞ using the selective frequency damping method (Åkervik *et al.* 2006). This solver technique essentially damps out any oscillation in the flow field using proportional feedback control with temporal filtering to force the flow to the unstable steady state. We note that this unstable steady state is not the time-averaged state, as shown for an example with $Re = 100$ and $M_\infty = 0$ in figure 10. The most immediately recognizable difference between the two flows is the sharp kink seen in the vorticity field of the time-averaged flow, which is absent from the smooth profile of the unstable steady state. Also, note that the unstable steady state for flow over a circular cylinder matches the steady symmetric profile examined by Fornberg (1980) for incompressible flow.

The present linear stability analysis is conducted by performing numerical simulation using the unstable steady state taken as the initial condition, with a small numerical perturbation introduced. We emphasize that while the simulation is performed with the full nonlinear Navier–Stokes equations, the nonlinear advection term is negligible for the level of perturbation considered. Furthermore, by limiting our focus to the time period just after the introduction of the perturbation, the magnitude of C_l is assumed to be sufficiently small to allow us to ignore the nonlinear term in (1.1). We thus perform the linear stability analysis by tracking the time evolution of the perturbation to the lift coefficient C_l through the linearized version of (1.1),

$$\frac{\mathrm{d}C_l}{\mathrm{d}t} = \sigma C_l, \tag{3.2}$$

for the dominant instability. The solution to this equation is

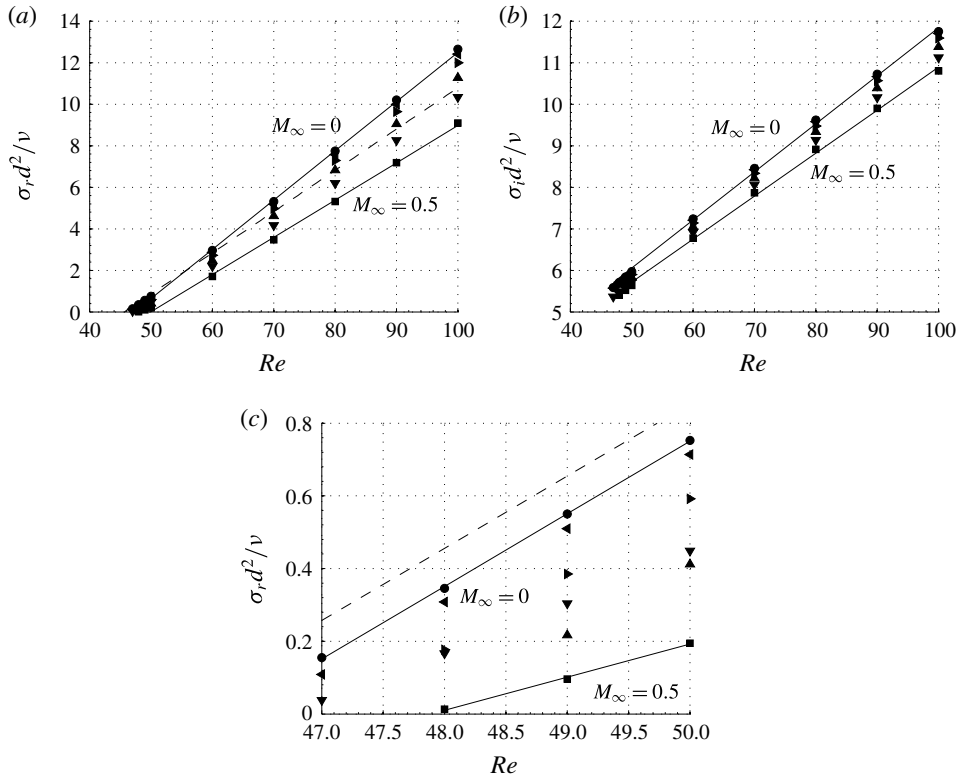$$C_l(t) = C_{l,t=0}\, \mathrm{e}^{\sigma t}, \tag{3.3}$$

FIGURE 11. (*a*) Growth rate $\sigma_r d^2/\nu$ and (*b*) dominant unstable frequency $\sigma_i d^2/\nu$ obtained for various M_∞ as functions of Re. Overlaid solid lines are linear curve fits of the present data (excluding observations at $Re < 50$), while the dashed line is taken from the incompressible flow data of Strykowski & Sreenivasan (1990). (*c*) The growth rate $\sigma_r d^2/\nu$ for $Re \leqslant 50$, with selected curve fits excluding observations at $Re > 50$: $\bullet$, $M_\infty = 0.0$; $\blacktriangleleft$, $M_\infty = 0.1$; $\blacktriangleright$, $M_\infty = 0.2$; $\blacktriangle$, $M_\infty = 0.3$; $\blacktriangledown$, $M_\infty = 0.4$; $\blacksquare$, $M_\infty = 0.5$.

where $C_{l,t=0}$ is the initial lift amplitude generated by a small perturbation (note that lift for the unstable steady state is zero). By fitting curves of the form given in (3.3) to C_l values computed during simulation, the growth rate $\sigma_r = \text{Re}(\sigma)$ and dominant unstable frequency $\sigma_i = \text{Im}(\sigma)$ are determined for the chosen Re and M_∞. This procedure, without the determination of the unstable steady state, has been used previously by Brés & Colonius (2008) for tracking the decay of disturbances for a linear stability analysis of compressible flow over open rectangular cavities.

For the growth rate of instabilities, we find that compressibility stabilizes the flow, as increasing M_∞ decreases σ_r. We also note that the critical Reynolds number Re_c increases with increasing M_∞. These trends can be seen in figure 11, which shows $\sigma_r d^2/\nu$ as a function of Re for various M_∞. Strykowski & Sreenivasan (1990) made experimental measurements of this quantity in a wind tunnel equipped with valves that allowed a rapid change in the wind tunnel velocity. By changing the velocity, Re was quickly changed from stable to unstable values and vice versa. Hot-wire anemometry and laser Doppler velocimetry recordings of streamwise velocity were then employed in the wake to show that, for incompressible flow, $\sigma_r d^2/\nu$ can be fitted with a function

of the form

$$\frac{\sigma_r d^2}{\nu} = \alpha Re + \beta, \tag{3.4}$$

where the term d^2/ν is the viscous time scale for each case. For their analysis, α and β were taken to be constants. The present data demonstrate that this correlation works well for Re above the predicted Re_c, and can also be applied to the non-dimensional dominant unstable frequency

$$\frac{\sigma_i d^2}{\nu} = \eta Re + \delta, \tag{3.5}$$

where η and δ are constants at a given M_∞. However, in both cases, the correlations show a slight deviation near Re_c. To illustrate this point, we perform curve fits of $\sigma_r d^2/\nu$ and $\sigma_i d^2/\nu$ as a function of Re at each M_∞, excluding observations made at $Re < 50$. Curve fits of the form given in (3.4) and (3.5) are presented for selected cases using solid lines in figure 11(a,b), and show that (3.4) and (3.5) slightly underpredict the growth rate for cases near Re_c.

We also observe from figure 11 that the present data for incompressible flow exhibit lower growth rates than those taken from Strykowski & Sreenivasan (1990) for most of the range of Re considered ($Re \gtrsim 55$). We attribute this discrepancy to differences in the experimental and numerical setups. While the flow in the present study is provided with a small perturbation at constant Re, the flow in the study undertaken by Strykowski & Sreenivasan (1990) had to be quickly altered from stable to unstable Re through a change in the wind tunnel velocity. The transient period resulting from this flow acceleration may explain the difference in growth rates, given that the observed difference increases with increasing Re (i.e. with greater flow acceleration in the wind tunnel). It should be further noted that the initial base state in the analysis performed by Strykowski & Sreenivasan (1990) is at a stable Re, whereas the present study is initialized from a base state with unstable Re.

The accuracy of (3.4) and (3.5) over most of the range of Re considered in this study motivates the creation of a similar equation that includes compressibility effects. Owing to the strong quadratic correlation between $\overline{C}_d$ and M_∞ previously observed in figure 5, similar quadratic functions were chosen as first approximations to the dependence of the slopes and intercepts of (3.4) and (3.5) on M_∞. Indeed, we find that both the slopes and the intercepts are well-predicted using a function of M_∞^2, as shown in figure 12. As such, the constants in (3.4) and (3.5) may be re-written to include compressibility effects:

$$\alpha = \alpha_2 M_\infty^2 + \alpha_0, \tag{3.6}$$
$$\beta = \beta_2 M_\infty^2 + \beta_0, \tag{3.7}$$
$$\eta = \eta_2 M_\infty^2 + \eta_0, \tag{3.8}$$
$$\delta = \delta_2 M_\infty^2 + \delta_0, \tag{3.9}$$

where the parameters on the right-hand side are taken to be constant over the range of M_∞ considered and are shown on figure 12. On substituting these equations into
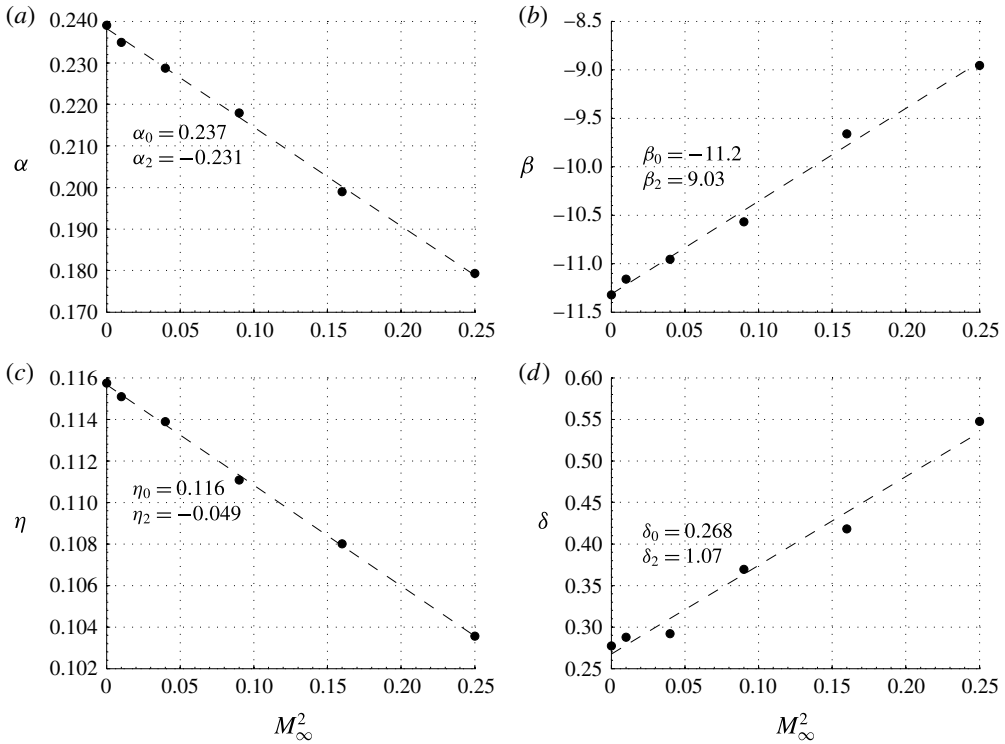
FIGURE 12. Slopes ($\alpha = \alpha_2 M_\infty^2 + \alpha_0$, $\eta = \eta_2 M_\infty^2 + \eta_0$) and intercepts ($\beta = \beta_2 M_\infty^2 + \beta_0$, $\delta = \delta_2 M_\infty^2 + \delta_0$) obtained from linear curve fits of $\sigma_r d^2/\nu = \alpha Re + \beta$ and $\sigma_i d^2/\nu = \eta Re + \delta$.

(3.4) and (3.5) one obtains

$$\frac{\sigma_r d^2}{\nu} = (\alpha_2 M_\infty^2 + \alpha_0)Re + (\beta_2 M_\infty^2 + \beta_0), \tag{3.10}$$

$$\frac{\sigma_i d^2}{\nu} = (\eta_2 M_\infty^2 + \eta_0)Re + (\delta_2 M_\infty^2 + \delta_0), \tag{3.11}$$

which enables us to predict the growth rate and dominant frequency of instabilities for two-dimensional compressible laminar flow. Again, it must be noted that these equations have only been validated for $50 \leqslant Re \leqslant 100$ and $M_\infty \leqslant 0.5$. We have also considered a separate set of curve fits for observations made at $Re \leqslant 50$ using the same procedure. In this manner, it would be possible to create piecewise functions capable of predicting the growth rates and frequencies over the entire range of Re and M_∞ considered. Indeed, it was found that the data were well-described by equations of the form given in (3.4) and (3.5), and selected curve fits are overlaid in figure 11(c). However, as illustrated in that figure, there was a sudden increase in the growth rate from $M_\infty = 0.3$ to 0.4. As such, it appears that a naïve curve fit as a function of M_∞^2, as in (3.6)–(3.9), would not fully capture the transition.

The impact of compressibility on the frequency of oscillations during the linear growth stage (measured by σ_i) can be observed in figure 13. From this plot, we see that as Re increases, the frequency of oscillations increases from the linear growth
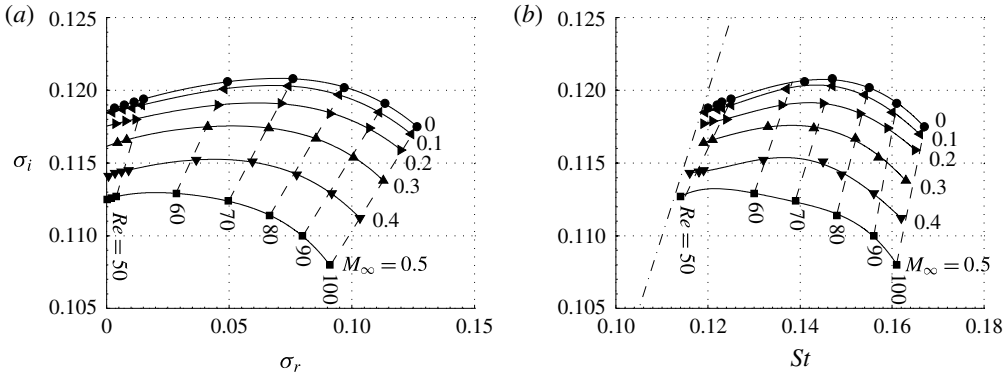
FIGURE 13. (*a*) Dominant unstable frequency σ_i obtained for various M_∞ as functions of σ_r. (*b*) Comparison of σ_i and St for various M_∞. Reference line (dashed-dotted) corresponds to $\sigma_i = St$.
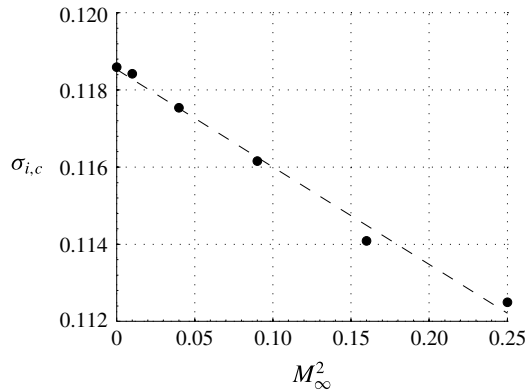

FIGURE 14. Critical dominant frequency $\sigma_{i,c} = \sigma_i|_{\sigma_r=0}$ as a function of M_∞^2.

stage to the saturated nonlinear oscillatory flow. This result is not unexpected, since it is well-established that the frequency of instabilities increases in conjunction with Re for the range considered. However, for fixed Re and increasing M_∞, we also observe that the frequency of oscillations in the linear growth stage decreases. This trend matches that previously discussed for flows in the nonlinear, saturated stage (figure 8). Furthermore, over the range of M_∞ considered in this study, we find that the change in σ_i relative to its incompressible value remains relatively constant with increasing Re. By contrast, the relative change in St over the range of M_∞ considered becomes smaller as Re increases, as previously discussed in the context of figure 8.

Interestingly, the critical dominant frequencies $\sigma_{i,c}$ (i.e. σ_i when $\sigma_r = 0$) predicted by the lines given on figure 13(*a*) seem to exhibit a quadratic relationship with M_∞, as displayed in figure 14. This relationship holds despite the fact that the lines take into account growth rates for which $(Re - Re_c) < 5$, a condition that we observed to result in deviations from the linear correlation between $\sigma_r d^2/\nu$ and Re presented in (3.4).

Finally, the data used in this work are provided in appendix A. Tables 4 and 5 summarize the wake characteristics behind a circular cylinder for compressible viscous

Re	M_∞	C_d	l_a/d	l_b/d	l_r/d	θ_s (deg.)
20	0	2.07	0.356	0.425	0.921	43.7
	0.1	2.09	0.356	0.425	0.922	43.7
	0.2	2.08	0.358	0.426	0.928	43.7
	0.3	2.11	0.362	0.428	0.940	43.7
	0.4	2.16	0.365	0.429	0.954	43.6
	0.5	2.23	0.367	0.428	0.963	43.4
40	0	1.54	0.715	0.594	2.24	53.8
	0.1	1.54	0.718	0.594	2.25	53.7
	0.2	1.56	0.724	0.596	2.28	53.7
	0.3	1.58	0.736	0.602	2.34	53.7
	0.4	1.62	0.752	0.609	2.43	53.5
	0.5	1.68	0.769	0.614	2.53	53.3

TABLE 4. Steady wake characteristics behind a circular cylinder for compressible viscous flow at representative Reynolds numbers of 20–40.

flow at representative Reynolds numbers of 20–60 and 70–100, respectively. Table 6 lists the linear growth rates and frequencies for instabilities with respect to the compressible unstable steady states around a circular cylinder.

4. Conclusion

The present study employs DNS to examine the two-dimensional viscous compressible flow around a circular cylinder. In comparing flow-field characteristics, interesting similarities are shown between stable and unstable cases. In both regimes, it is found that increasing the free-stream Mach number increases $\overline{C_d}$. This result is expected, and reflects results from other studies at higher Re (Lindsey 1937; Macha 1977). For cases below the critical Reynolds number for two-dimensional shedding, it is found that compressibility effects elongate the wake and cause a small delay in flow separation. Likewise, for unstable cases, increasing the free-stream Mach number results in a larger time-averaged recirculation region and vortex-shedding wavelength. Furthermore, as Re is decreased for stable flows, the wake geometry is observed to exhibit a smaller variation over the range of free-stream Mach numbers considered. In a similar fashion, for unstable flows, though the non-dimensional shedding frequency decreases monotonically with increasing free-stream Mach number at every Re studied, the magnitude of this decrease shrinks as Re increases. These similarities in behaviour between stable and unstable flows suggest that the difference between Re and the critical Reynolds number for the emergence of two-dimensional shedding plays a significant role in determining the sensitivity of a flow to compressibility effects.

Through a linear stability analysis, the growth rate and frequency of the primary wake instability that arises for Re above the critical value are examined. In doing so, it is found that the non-dimensional growth rate of the primary wake instability exhibits a linear correlation with Re at every free-stream Mach number considered. Moreover, the variation in the curve fitting parameters for correlations at different free-stream Mach numbers are found to be well-explained by a dependence on the square of the Mach number. Additionally, it is observed that at a given Re, the growth rate decreases with increasing free-stream Mach number. This trend is also observed

Re	M_∞	C_d	C_l	St
50	0	1.44 ± 0.00160	± 0.0561	0.126
	0.1	1.45 ± 0.00155	± 0.0546	0.125
	0.2	1.46 ± 0.00122	± 0.0486	0.124
	0.3	1.46 ± 0.00115	± 0.0399	0.121
	0.4	$1.52 \pm 4.53 \times 10^{-5}$	± 0.0314	0.119
	0.5	$1.56 \pm 2.03 \times 10^{-5}$	± 0.0144	0.114
60	0	1.41 ± 0.00105	± 0.132	0.141
	0.1	1.416 ± 0.00105	± 0.132	0.137
	0.2	1.427 ± 0.00095	± 0.125	0.136
	0.3	1.453 ± 0.0009	± 0.118	0.133
	0.4	1.4925 ± 0.00065	± 0.112	0.132
	0.5	1.5510 ± 0.0005	± 0.091	0.130
70	0	1.383 ± 0.0023	± 0.190	0.147
	0.1	1.392 ± 0.0025	± 0.194	0.147
	0.2	1.403 ± 0.0024	± 0.186	0.145
	0.3	1.430 ± 0.0022	± 0.178	0.143
	0.4	1.503 ± 0.0056	± 0.230	0.145
	0.5	1.535 ± 0.0013	± 0.156	0.139
75	0	1.37 ± 0.00313	± 0.216	0.151
	0.1	1.38 ± 0.00336	± 0.217	0.150
	0.2	1.39 ± 0.00310	± 0.212	0.150
	0.3	1.42 ± 0.00288	± 0.205	0.148
	0.4	1.47 ± 0.00356	± 0.210	0.147
	0.5	1.53 ± 0.00214	± 0.190	0.144
80	0	1.364 ± 0.0040	± 0.240	0.155
	0.1	1.373 ± 0.0040	± 0.239	0.154
	0.2	1.385 ± 0.0041	± 0.238	0.153
	0.3	1.413 ± 0.0040	± 0.234	0.152
	0.4	1.466 ± 0.0045	± 0.230	0.149
	0.5	1.525 ± 0.0024	± 0.222	0.148
90	0	1.350 ± 0.0065	± 0.286	0.161
	0.1	1.359 ± 0.0065	± 0.286	0.160
	0.2	1.373 ± 0.0059	± 0.286	0.159
	0.3	1.404 ± 0.0066	± 0.286	0.157
	0.4	1.452 ± 0.0056	± 0.284	0.156
	0.5	1.541 ± 0.0090	± 0.279	0.156
100	0	1.34 ± 0.0091	± 0.329	0.167
	0.1	1.35 ± 0.0096	± 0.328	0.166
	0.2	1.36 ± 0.0093	± 0.332	0.165
	0.3	1.39 ± 0.0086	± 0.326	0.163
	0.4	1.45 ± 0.0086	± 0.328	0.162
	0.5	1.54 ± 0.0101	± 0.352	0.161

TABLE 5. Unsteady wake characteristics behind a circular cylinder for compressible viscous flow at representative Reynolds numbers of 50–100.

Re	M_∞	σ_r	σ_i
47	0	3.037×10^{-3}	0.1188
	0.1	2.319×10^{-3}	0.1185
	0.4	7.963×10^{-4}	0.1141
48	0	7.196×10^{-3}	0.1190
	0.1	6.418×10^{-3}	0.1187
	0.2	3.681×10^{-3}	0.1177
	0.4	3.456×10^{-3}	0.1143
	0.5	2.662×10^{-4}	0.1125
49	0	1.123×10^{-2}	0.1192
	0.1	1.041×10^{-2}	0.1188
	0.2	7.854×10^{-3}	0.1179
	0.3	4.436×10^{-3}	0.1164
	0.4	6.193×10^{-3}	0.1144
	0.5	1.964×10^{-3}	0.1126
50	0	1.505×10^{-2}	0.1194
	0.1	1.428×10^{-2}	0.1190
	0.2	1.184×10^{-2}	0.1180
	0.3	8.232×10^{-3}	0.1166
	0.4	8.974×10^{-3}	0.1145
	0.5	3.894×10^{-3}	0.1127
60	0	4.931×10^{-2}	0.1206
	0.1	4.790×10^{-2}	0.1201
	0.2	4.536×10^{-2}	0.1190
	0.3	4.123×10^{-2}	0.1175
	0.4	3.651×10^{-2}	0.1152
	0.5	2.844×10^{-2}	0.1129
70	0	7.595×10^{-2}	0.1208
	0.1	7.409×10^{-2}	0.1203
	0.2	7.102×10^{-2}	0.1191
	0.3	6.610×10^{-2}	0.1174
	0.4	5.941×10^{-2}	0.1151
	0.5	4.964×10^{-2}	0.1124
80	0	9.686×10^{-2}	0.1202
	0.1	9.469×10^{-2}	0.1197
	0.2	9.111×10^{-2}	0.1184
	0.3	8.536×10^{-2}	0.1167
	0.4	7.744×10^{-2}	0.1142
	0.5	6.640×10^{-2}	0.1114

TABLE 6. Continued on next page.

for the dominant unstable frequency and the non-dimensional shedding frequency, hence indicating that compressibility effects tend to stabilize the flow. Finally, it is seen that as *Re* approaches its critical value, the non-dimensional shedding frequency approaches the dominant unstable frequency. This behaviour suggests that as *Re* nears the critical Reynolds number, the saturated flow characteristics increasingly depend

90	0	1.134×10^{-1}	0.1191
	0.1	1.110×10^{-1}	0.1185
	0.2	1.071×10^{-1}	0.1174
	0.3	1.006×10^{-1}	0.1154
	0.4	9.174×10^{-2}	0.1129
	0.5	7.976×10^{-2}	0.1100
100	0	1.265×10^{-1}	0.1175
	0.1	1.241×10^{-1}	0.1170
	0.2	1.199×10^{-1}	0.1159
	0.3	1.128×10^{-1}	0.1138
	0.4	1.033×10^{-1}	0.1112
	0.5	9.095×10^{-2}	0.1080

TABLE 6 (cntd). Linear growth rates and frequencies for instabilities with respect to compressible unstable steady states around a circular cylinder.

on the characteristics of the dominant unstable mode in the linear growth stage. This result, coupled with the previous observation that the flow also becomes more sensitive to compressibility effects as *Re* approaches the critical value, suggests that the dominant unstable mode is sensitive to changes in the free-stream Mach number.

Acknowledgements

Appendix

This appendix contains the data presented in this paper tabulated as tables 4–6.

REFERENCES

ÅKERVIK, E., BRANDT, L., HENNINGSON, D. S., HŒPFFNER, J., MARXEN, O. & SCHLATTER, P. 2006 Steady solutions of the Navier–Stokes equations by selective frequency damping. *Phys. Fluids* **18**, 068102.

BEHARA, S. & MITTAL, S. 2010 Wake transition in flow past a circular cylinder. *Phys. Fluids* **22**, 114104.

BÉNARD, H. 1908 Formation de centres de giration à l'arrière d'un obstacle en mouvemènt. *C. R. Acad. Sci.* **147**, 839–842.

BIRD, G. A. 1994 *Molecular Gas Dynamics and the Direct Simulation of Gas Flows*. Oxford University Press.

BISHOP, R. E. D. & HASSAN, A. Y. 1964 The lift and drag forces on a circular cylinder in a flowing fluid. *Proc. R. Soc. Lond.* A **277** (1368), 32–50.

BRÉS, G. A. & COLONIUS, T. 2008 Three-dimensional instabilities in compressible flow over open cavities. *J. Fluid Mech.* **599**, 309–339.

BRÉS, G. A., NICHOLS, J. W., LELE, S. K. & HAM, F. E. 2012 Towards best practices for jet noise predictions with unstructured large eddy simulations. In *42nd AIAA Fluid Dynamics Conference New Orleans*.

COUTANCEAU, M. & BOUARD, R. 1977 Experimental determination of the main features of the viscous flow in the wake of a circular cylinder in uniform translation. Part 1. Steady flow. *J. Fluid Mech.* **79** (2), 231–256.

DELANY, N. K. & SORENSON, N. S. 1953 Low-speed drag of cylinders of various shapes. *NACA Tech. Rep.* 3038.

DRELA, M. 1992 Transonic low-Reynolds number airfoils. *J. Aircraft* **29** (6), 1106–1113.

DUŠEK, J., LE GAL, P. & FRAUNIÉ, P. 1994 A numerical and theoretical study of the first Hopf bifurcation in a cylinder wake. *J. Fluid Mech.* **264**, 59–80.

FINN, R. K. 1953 Determination of the drag on a cylinder at low Reynolds numbers. *J. Appl. Phys.* **24** (6), 771–773.

FORNBERG, B. 1980 A numerical study of steady viscous flow past a circular cylinder. *J. Fluid Mech.* **98**, 819–855.

FREUND, J. B. 1997 Proposed inflow/outflow boundary condition for direct computation of aerodynamic sound. *AIAA J.* **35** (4), 740–742.

FUNG, Y. C. 1960 Experiments on the flow past a circular cylinder at very high Reynolds number. *J. Aero. Space Sci.* **27**, 801–814.

GERRARD, J. H. 1961 An experimental investigation of the oscillating lift and drag of a circular cylinder shedding turbulent vortices. *J. Fluid Mech.* **11** (2), 244–256.

GIANNETTI, F. & LUCHINI, P. 2007 Structural sensitivity of the first instability of the cylinder wake. *J. Fluid Mech.* **581**, 167–197.

GLAUERT, H. 1928 The effect of compressibility on the lift of an aerofoil. *Proc. R. Soc. Lond.* A **118** (779), 113–119.

GOROKHOVSKI, M. & HERRMANN, M. 2008 Modeling primary atomization. *Annu. Rev. Fluid Mech.* **40**, 343–366.

KARAGIOZIS, K., KAMAKOTI, R. & PANTANO, C. 2010 A low numerical dissipation immersed interface method for the compressible Navier–Stokes equations. *J. Comput. Phys.* **229**, 701–727.

VON KÁRMÁN, T. 1911 Über den mechanismus des widerstandes, den ein bewegter körper in einer flußseigkeit afahrt. *Gott. Nachr.* 509–517.

KHALIGHI, Y., NICHOLS, J. W., HAM, F., LELE, S. K. & MOIN, P. 2011 Unstructured large eddy simulation for prediction of noise issued from turbulent jets in various configurations. In *17th AIAA/CEAS Aeroacoustics Conference*.

KUMAR, B., KOTTARAM, J. J., SINGH, A. K. & MITTAL, S. 2009 Global stability analysis of flow past a cylinder with centerline symmetry. *J. Fluid Mech.* **632**, 273–300.

LINDSEY, W. F. 1937 Drag of cylinders of simple shapes. *NACA Tech. Rep.* 619.

LINNICK, M. N. & FASEL, H. F. 2005 A high-order immersed interface method for simulating unsteady incompressible flows on irregular domains. *J. Comput. Phys.* **204**, 157–192.

MACHA, J. M. 1977 Drag of circular cylinders at transonic Mach numbers. *J. Aircraft* **14**, 605–607.

MALLOCK, A. 1907 On the resistance of air. *Proc. R. Soc. Lond.* A **79**, 262–265.

MARSDEN, J. E. & MCCRACKEN, M. 1976 *The Hopf Bifurcation and Its Applications*, Applied Mathematical Sciences, vol. 19. Springer.

MEIRON, D. I., SAFFMAN, P. G. & SCHATZMAN, J. C. 1984 The linear two-dimensional stability of inviscid vortex streets of finite-cored vortices. *J. Fluid Mech.* **147**, 187–212.

MUNDAY, P. M., TAIRA, K., SUWA, T., NUMATA, D. & ASAI, K. 2015 Nonlinear lift on a triangular airfoil in low-Reynolds-number compressible flow. *J. Aircraft* **52** (3), 924–931.

NAGAI, H., ASAI, K., NUMATA, D. & SUWA, T. 2013 Characteristics of low-Reynolds number airfoils in a Mars wind tunnel. *AIAA Paper* 2013-0073.

NOACK, B. R., AFANASIEV, K., MORZYNSKI, M., TADMOR, G. & THIELE, F. 2003 A hierarchy of low-dimensional models for the transient and post-transient cylinder wake. *J. Fluid Mech.* **497**, 335–363.

NORBERG, C. 2001 Flow around a circular cylinder: aspects of fluctuating lift. *J. Fluids Struct.* **15** (3), 459–469.

OKAMOTO, M. 2005 An experimental study in aerodynamic characteristics of steady and unsteady airfoils at low Reynolds number. PhD thesis, Nihon University.

PROVANSAL, M., MATHIS, C. & BOYER, L. 1987 Bénard–von Kármán instability: transient and forced regimes. *J. Fluid Mech.* **182**, 1–22.

RAYLEIGH, LORD 1879 Acoustical observations. *Phil. Mag. J. Sci.* **7** (42), 149–162.

ROSHKO, A. 1954 On the development of turbulent wakes from vortex streets. *NACA Tech. Rep.* 1191.

ROSHKO, A. 1961 Experiments on the flow past a circular cylinder at very high Reynolds number. *J. Fluid Mech.* **10** (3), 345–356.

SAFFMAN, P. G. & SCHATZMAN, J. C. 1982 Stability of a vortex street of finite vortices. *J. Fluid Mech.* **117**, 171–185.

SANADA, S. & MATSUMOTO, S. 1992 Full scale measurements of wind force action on and response of a 200 m concrete chimney. *J. Wind Engng. Ind. Aerodyn.* **43**, 2165–2176.

SENGUPTA, T. K., SINGH, N. & SUMAN, V. K. 2010 Dynamical system approach to instability of flow past a circular cylinder. *J. Fluid Mech.* **656**, 82–115.

SHINJO, J. & UMEMURA, A. 2010 Simulation of liquid jet primary breakup: dynamics of ligament and droplet formation. *Intl J. Multiphase Flow* **36**, 513–532.

SIPP, D. & LEBEDEV, A. 2007 Global stability of base and mean flows: a general approach and its applications to cylinder and open cavity flows. *J. Fluid Mech.* **593**, 333–358.

STROUHAL, V. 1878 On one particular way of tone generation. *Ann. Phys. Leipzig* 3 **5**, 216–251.

STRYKOWSKI, P. J. & SREENIVASAN, K. R. 1990 On the formation and suppression of vortex 'shedding' at low Reynolds numbers. *J. Fluid Mech.* **218**, 71–107.

SUWA, T., NOSE, K., NUMATA, D., NAGAI, H. & ASAI, K. 2012 Compressibility effects on airfoil aerodynamics at low Reynolds number, *AIAA Paper* 2012-3029.

TAIRA, K. & COLONIUS, T. 2007 The immersed boundary method: a projection approach. *J. Comput. Phys.* **225**, 2118–2137.

TANEDA, S. 1956 Experimental investigation of the wakes behind cylinders and plates at low Reynolds numbers. *J. Phys. Soc. Japan* **11**, 302–307.

TRITTON, D. J. 1959 Experiments on the flow past a circular cylinder at low Reynolds number. *J. Fluid Mech.* **6**, 547–567.

WIESELSBERGER, C. VON 1921 Neuere feststellungen über die gesetze des flüssigkeits-und luftwiderstandes. *Phys. Z.* **22** (11), 321–328.

WILLIAMSON, C. H. K. 1988*a* Defining a universal and continuous Strouhal–Reynolds number relationship for the laminar vortex shedding of a circular cylinder. *Phys. Fluids* **31** (10), 2742–2744.

WILLIAMSON, C. H. K. 1988*b* The existence of two stages in the transition to three-dimensionality of a cylinder wake. *Phys. Fluids* **31**, 3165–3168.

WILLIAMSON, C. H. K. 1996 Vortex dynamics in the cylinder wake. *Annu. Rev. Fluid Mech.* **28**, 477–539.

ZDRAVKOVICH, M. M. 1997 *Flow Around Circular Cylinders: Fundamentals*, Oxford Science Publications, vol. 1. Oxford University Press.